# Isospin dependence of mass-distribution shape of fission fragments of Hg isotopes

A. V. Andreev,[1] G. G. Adamian,[1] N. V. Antonenko,[1] and A. N. Andreyev[2,3,4]
[1]*Joint Institute for Nuclear Research, 141980 Dubna, Russia*
[2]*Instituut voor Kern- en Stralingsfysica, KU Leuven, B-3001 Leuven, Belgium*
[3]*Department of Physics, University of York, York YO10 5DD, United Kingdom*
[4]*Advanced Science Research Center, Japan Atomic Energy Agency, Tokai-mura, Ibaraki 319-1195, Japan*
(Received 18 September 2013; published 25 October 2013)

Using an improved scission-point model, the mass distributions are calculated for induced fission of even Hg isotopes with mass numbers $A = 174$ to 196. With increasing $A$ of a fissioning $^{A}$Hg nucleus the mass distribution evolves from symmetric for $^{174}$Hg, to asymmetric for isotopes close to $^{180}$Hg, and back to more symmetric for $^{192,194,196}$Hg. In the fissioning Hg isotopes their excitation energy weakly influences the shape of the mass distribution. In $^{180,184}$Hg, the mass distributions of fission fragments remain asymmetric even at high excitation energies.

DOI: 10.1103/PhysRevC.88.047604 PACS number(s): 24.75.+i, 25.85.−w, 24.10.Pa

An interest in the theoretical exploration of fission process was restimulated several years ago after the experiment on $\beta$-delayed fission of $^{180}$Tl [1,2], where the mass distribution of fission fragments of post-$\beta$-decay daughter nucleus $^{180}$Hg was found to be asymmetric. This was surprising since from a native point of view the mass distributions were expected to be symmetric for nuclei lighter than thorium. In the earlier experiments on fission of Au-Po nuclei [3], a weak asymmetry of the mass distributions was observed as well, but the deviations of these distributions from the Gaussian were found to be rather small. The experiment [1] was followed by several theoretical works describing the observed asymmetric shape of the fission-fragment mass distribution [4–7]. The existing experimental data on the fission of $^{180}$Hg and $^{198}$Hg were well described with our improved scission-point model [4]. In the previous study we found that the asymmetry of the shape of mass distribution decreases with increasing mass number $A$ of the fissioning even $^{A}$Hg nucleus from $A = 180$ to $A = 198$. However, the fissions of the Hg isotopes lighter than $^{180}$Hg were not covered in our previous treatment. In the study of low-energy fission of neutron-deficient mercury isotopes with the Brownian Metropolis shape-motion treatment [5], the mass distribution is found to be symmetric for $^{174}$Hg and becomes asymmetric with growing mass number of the fissioning mercury isotope to $^{180}$Hg. The present work is an extension of our previous calculations [4] to a wider range of Hg isotopes in order to reveal the dependence of the shape of fission-fragment mass distribution on the mass number $A$ and excitation energy $E^*_{CN}(l = 0)$ of the fissioning $^{A}$Hg isotope and to compare the results obtained with those of other theoretical models. Here, $l$ is the angular momentum of the fissioning nucleus.

We describe the fission observables within the improved scission-point model [4,8] which operates with the relative probabilities of formation of different scission configurations obtained with the statistical approach by calculating the potential energy of scission configurations. At the scission point the fissioning nucleus is modeled by a dinuclear system consisting of two nearly touching prolate coaxial spheroids with deformation parameters defined as the ratios of the major and minor semiaxes of the spheroids $\beta_i = c_i/a_i$, where $i = L, H$ denotes light and heavy fragments of the dinuclear system, respectively. The mass and charge numbers of the fragments are $A_i$ and $Z_i$, respectively. $A = A_L + A_H$ and $Z = Z_L + Z_H$ are the mass and charge numbers of the fissioning nucleus, respectively. The potential energy

$$\begin{aligned} &U(A_i, Z_i, \beta_i, R, l) \\ &= U_L^{LD}(A_L, Z_L, \beta_L) + \delta U_L^{\text{shell}}(A_L, Z_L, \beta_L) \\ &\quad + U_L^{zpv}(A_L, Z_L) + U_H^{LD}(A_H, Z_H, \beta_H) \\ &\quad + \delta U_H^{\text{shell}}(A_H, Z_H, \beta_H) + U_H^{zpv}(A_H, Z_H) \\ &\quad + V^C(A_i, Z_i, \beta_i, R) + V^N(A_i, Z_i, \beta_i, R) \\ &\quad + V^{\text{rot}}(A_i, Z_i, \beta_i, R, l) \end{aligned} \tag{1}$$

of the dinuclear system consists of the energies of the fragments, energy of their interaction, and rotational energy $V^{\text{rot}}$ in the case of induced fission. The energy of each fragment consists of the liquid-drop energy $U_i^{LD}$, deformation dependent shell-correction term $\delta U_i^{\text{shell}}$, and the energy of the zero-point vibrations $U_i^{zpv} = E_i^{2^+} \coth[E_i^{2^+}/T(l)]$, associated with the energy $E_i^{2^+}$ of the first $2^+$ excited state. The damping of the shell corrections with temperature is introduced in order to take into account the influence of the excitation energy. The interaction potential consists of the Coulomb interaction potential $V^C$ of the two uniformly charged spheroids and nuclear interaction potential $V^N$ in the form of a double folding of Woods-Saxon nuclear densities of the fragments and Skyrme-type density-dependent nucleon-nucleon interaction. The interaction potential has a pocket at a distance between the tips of the fragments of about 0.5 to 1 fm (in the considered region of fissioning nuclei) depending on deformations of the fragments. The internuclear distance $R$ in (1) corresponds to the position of this pocket (minimum) $R = R_m(\beta_i)$. The excitation energy $E^*(A_i, Z_i, \beta_i, R_m, l)$ at the scission is calculated as the initial excitation energy of the fissioning nucleus plus the difference between the potential energies of the fissioning nucleus and the dinuclear system at the scission point. The details of the calculations of the potential energy are given in Ref. [4].

 

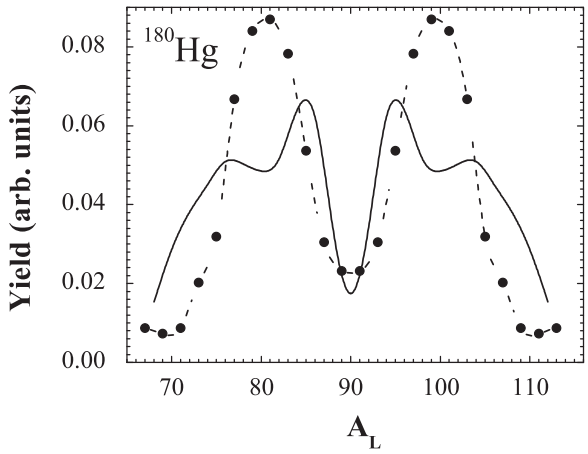


FIG. 1. Calculated (solid line) and experimental [2] (points connected by dashed line) mass distributions of fission fragments for $\beta$-delayed fission of $^{180}$Tl (fissioning nucleus is $^{180}$Hg).

The relative formation probability of the dinuclear system with particular masses, charges, and deformations of the fragments is calculated within the statistical approach as follows:

$$Y(A_i, Z_i, \beta_i, l) \sim \exp\left\{-\frac{U(A_i, Z_i, \beta_i, l)}{T(l)}\right\}. \quad (2)$$

The temperature is $T(l) = \sqrt{E_l^*/a}$, where $E_l^* = \max[\{E^*(A_i, Z_i, \beta_i, R_m, l)\}]$ and $a = A/12$ is the level density parameter. In order to obtain the mass distribution in the fission of a particular nucleus with the mass number $A$ and charge number $Z$, one should integrate (2) over $Z_L$, $\beta_L$, and $\beta_H$, sum over $l$, and take into account that $A_L + A_H = A$ and $Z_L + Z_H = Z$. Finally, for the calculation of the mass distribution the following expression is obtained:

$$Y(A_L) = \frac{\sum_{l=0}^{l_{\max}}(2l+1)\int \exp\left\{-\frac{U(A_i,Z_i,\beta_i,l)}{T(l)}\right\} dZ_L d\beta_L d\beta_H}{\sum_{l=0}^{l_{\max}}(2l+1)\int \exp\left\{-\frac{U(A_i,Z_i,\beta_i,l)}{T(l)}\right\} dA_L dZ_L d\beta_L d\beta_H}. \quad (3)$$

This distribution is normalized to unity. The value of the angular momentum $l$ is limited by either the kinetic angular momentum $l_{\rm kin} = R_b\sqrt{2\mu(E_{\rm c.m.} - V_b)}$ [$R = R_b$ is the position of the Coulomb barrier with the height $V_b = V^C(A_i, Z_i, \beta_i = 0, R = R_b) + V^N(A_i, Z_i, \beta_i = 0, R = R_b)$ in the entrance channel, $\mu = m_0 A_L A_H/(A_L + A_H)$ is the reduced mass parameter, and $m_0$ is the nucleon mass] or by the calculated critical angular momentum $l_{cr}$ in the entrance channel, depending on which one is smaller: $l_{\max} = \min\{l_{\rm kin}, l_{cr}\}$.

For a comparison with the recent experimental data [2], we performed the calculations for the fission of the post-$\beta$-decay daughter nucleus $^{180}$Hg with the excitation energy of $E^*_{CN}(l = 0) = 10.44$ MeV (Fig. 1). As in the experiment [2], we obtained an asymmetric fission-fragment mass distribution. In Fig. 1, more experimental points are shown than in the corresponding figure of Ref. [4]. The calculated average mass of the light fragment is $\overline{A_L} = 79$ and the width of the mass distribution is $\sigma_{A_L} = 5$. The Total Kinetic Energy (TKE) was calculated by assuming that all the interaction energy at the scission point is transformed into the kinetic energy after a large separation of the fission fragments. The average value $\overline{\rm TKE} = 136$ MeV is found to be in good agreement with the experimental observation.

To reveal the dependence of the shape of the fission-fragment mass distribution on the mass of the fissioning Hg isotope, we treated the isotopes $^{174-196}$Hg with even mass numbers at zero angular momentum $l = 0$. The calculations were performed at the excitation energies 2 and 20 MeV above the fission barriers. The results are presented in Figs. 2 and 3. For $^{174}$Hg, the fission-fragment mass distribution is symmetric. With increasing mass number of Hg the asymmetry appears and becomes maximal for $^{180,182}$Hg. From $^{182}$Hg to $^{190}$Hg the dip at the symmetric mass division remains, but the asymmetry becomes smaller due to the decrease of the width of the distribution. From $^{190}$Hg to $^{196}$Hg the distribution remains narrow and the dip at the symmetric mass division diminishes. This result slightly differs from that of Ref. [5], where the mass distribution was found to be asymmetric as well for $^{180-188}$Hg, but the asymmetry increases with the mass number of the fissioning Hg isotope. In our calculations (Figs. 2 and 3), the asymmetry of the mass distribution decreases with increasing excitation of the fissioning Hg isotopes. This is in contrast to the results of Ref. [5] where the asymmetry of the fission-fragment mass distribution increases with the excitation energy in $^A$Hg with $A < 180$.

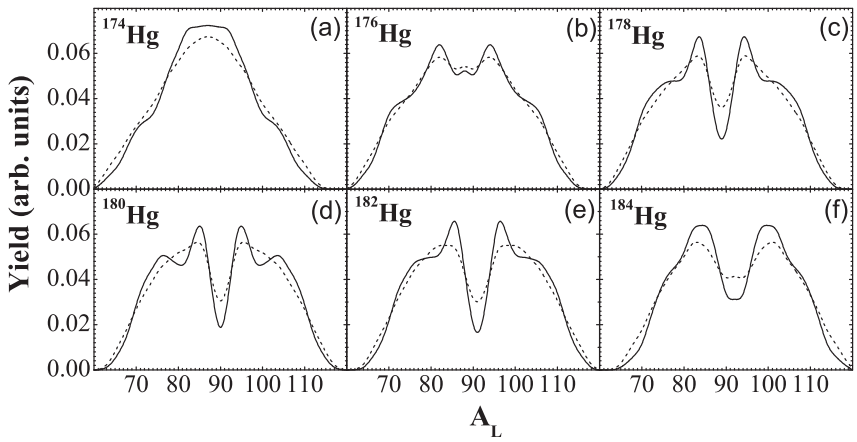


FIG. 2. Calculated mass distributions for the fission of (a) $^{174}$Hg, (b) $^{176}$Hg, (c) $^{178}$Hg, (d) $^{180}$Hg, (e) $^{182}$Hg, and (f) $^{184}$Hg at $l = 0$ and excitation energies of 2 (solid lines) and 20 MeV (dashed lines) above the corresponding fission barriers.

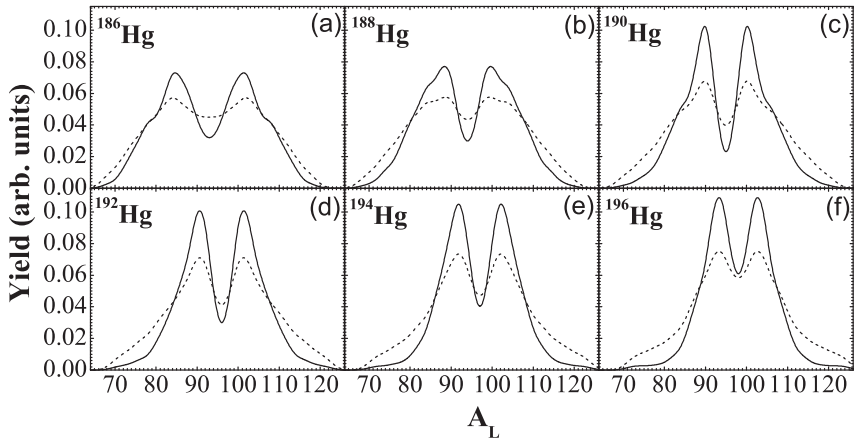


FIG. 3. The same as in Fig. 2, but for the fission of (a) $^{186}$Hg, (b) $^{188}$Hg, (c) $^{190}$Hg, (d) $^{192}$Hg, (e) $^{194}$Hg, and (f) $^{196}$Hg.

In order to explain the evolution of the shape of the fission-fragment mass distribution calculated, one can analyze the dependence of the potential energy on the deformations of the fragments at the scission point. As known, the shell effects are responsible for the appearance of the asymmetric mass distributions. Because of the strong Coulomb repulsion and, correspondingly, of the large polarization of nuclei, the potential energy (1) always has a minimum at deformations of the fission fragments of about $\beta_i = 1.5$ to 1.8, that is larger than their ground state deformations. Hence, the shell effects at large deformations mostly influence the shape of the fission-fragment mass distribution. The shell effects in nuclei near the ground state play a minor role if they are not very strong. The shell effects in nuclei around semimagic $^{90}$Zr are certainly weaker than in the nuclei around doubly magic tin and lead.

In the vicinity of the symmetric mass division of $^{180}$Hg, the shell corrections in the fragments close to the semimagic nucleus $^{90}$Zr are negative at small deformations, but at larger deformations, around the liquid-drop minimum of the potential energy, the shell corrections are positive and comparable with the shell corrections for the asymmetric split $^{76}$Ge + $^{104}$Pd [4]. As a result, the asymmetric prescission configuration can have a smaller potential energy due to a smaller nucleus-nucleus interaction. That is why the presence of magic fragments does not lead to a large yield of symmetric mass split in the fission of $^{180}$Hg. However, for the symmetric scission configuration the rigidity of the $^{90}$Zr nucleus leads to a very narrow minimum on the potential energy surface as a function of fragment deformations (see [4]). Due to the integration in (3), this narrow minimum leads to the reduction of the probability of a symmetric mass split. In contrast, for the asymmetric mass split of $^{180}$Hg, the potential energy as a function of fragment deformations has a wide minimum. The other factor, which suppresses the symmetric mass split in the fission of $^{180}$Hg and nearby isotopes, is rather large values of $E_i^{2^+}$ around $^{90}$Zr contributing to the terms $U_L^{zpv} + U_H^{zpv}$ in (1). All the factors mentioned above result in the asymmetric shape of the mass distribution in the fission of $^{180}$Hg and nearby isotopes.

In the isotopes of mercury lighter than $^{180}$Hg, the shell effects become rather weak and the values of $E_i^{2^+}$ become comparable for all mass divisions. Therefore, the shape of the fission-fragment mass distribution is defined by the liquid-drop part of the potential energy that leads to the symmetric mass distributions. For the region of heavier mercury isotopes, the influence of the shell effects at the symmetric mass split Zr + Zr is not so strong as in the $^{90}$Zr +$^{90}$ Zr case. However, the subshell at proton number $Z = 40$ for Zr results in a dip at a symmetric mass split similar to that in $^{180}$Hg [4].

In the region of mass numbers $A = 180$ to 200, one can find nuclei with comparable yields of symmetric and asymmetric fission modes. The mass distributions of fission fragments for these nuclei are expected to be very wide. In the fission of the $^{196}$Po nucleus, which is of the present experimental interest, we expect the comparable yields of symmetric and asymmetric fission modes.

To study the influence of bombarding energy (excitation energy and angular momentum) on the shape of the fission-fragment mass distribution, we consider the reactions $^{36}$Ar + $^{144}$Sm $\rightarrow$ $^{180}$Hg at bombarding energies in the center of mass 128 ($l_{\max} = 18$), 136 ($l_{\max} = 44$), 152 ($l_{\max} = 61$), 176 ($l_{\max} = 61$), and 200 MeV ($l_{\max} = 61$) and $^{40}$Ar + $^{144}$Sm $\rightarrow$ $^{184}$Hg at $E_{\text{c.m.}} = 125.2$ ($l_{\max} = 11$), 133 ($l_{\max} = 42$), 148.7 ($l_{\max} = 71$), 172.2 ($l_{\max} = 71$), and 195.6 MeV ($l_{\max} = 71$) (Figs. 4 and 5).

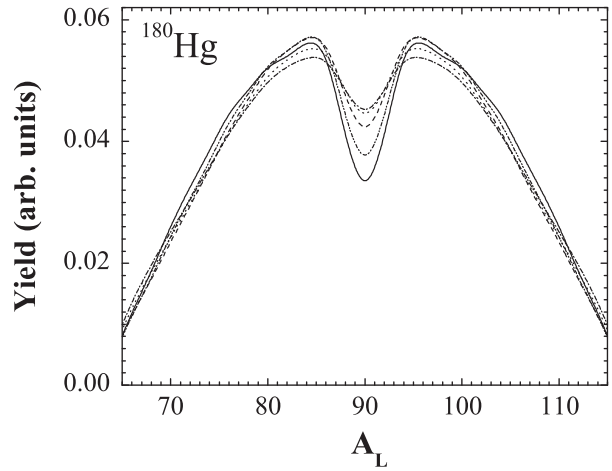


FIG. 4. Calculated mass distributions for the fission of $^{180}$Hg with the excitation energies of compound nucleus $E^*_{CN}(l = 0) = 36$ (solid line), 44 (dashed-dotted-dotted line), 60 (dashed line), 84 (dotted line), and 108 MeV (dashed-dotted line).

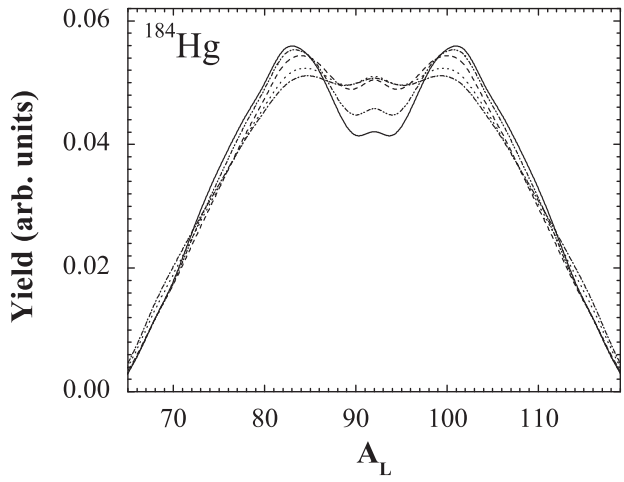


FIG. 5. Calculated mass distributions for the fission of $^{184}$Hg with the excitation energies of compound nucleus $E^*_{CN}(l = 0) = 34.5$ (solid line), 42.2 (dashed-dotted-dotted line), 58 (dashed line), 81.5 (dotted line), and 105 MeV (dashed-dotted line).

For the $^{36}$Ar + $^{144}$Sm ($^{40}$Ar + $^{144}$Sm) reaction, the bombarding energy $E_{\text{c.m.}} = 128$ MeV (125.2 MeV) corresponds to the excitation energy of the compound nucleus $E^*_{CN}(l = 0) =$ 36 MeV (34.5 MeV). Because the zero-point vibration effects are slowly reduced with increasing excitation energy, the mass distribution of the fission fragments of nuclei $^{180}$Hg ($^{184}$Hg) has a pronounced asymmetric shape even at high excitation energy $E^*_{CN}(l = 0) = 108$ MeV or $E^*_{CN}(l = l_{\max}) = 101$ MeV [$E^*_{CN}(l = 0) = 105$ MeV or $E^*_{CN}(l = l_{\max}) = 96$ MeV]. It is interesting to stress that the experimental mass distribution of the fragments in the fission of post-$\beta$-decay daughter nucleus $^{180}$Hg has a similar shape as the calculated mass distribution of the products in the $^{36}$Ar + $^{144}$Sm reaction. At high angular momenta some dinuclear scission configurations are energetically more favorable than the compound nucleus configuration and the fissionlike fragments in the $^{36}$Ar($E_{\text{c.m.}} =$ 152 to 200 MeV) + $^{144}$Sm reaction can be mainly produced by quasifission (but not by a fusion-fission process) [9].

The improved scission-point model [4,8] provides a good description of the experimental data on fission of $^{180}$Hg as well as of $^{198}$Hg (see [4]). In our model, the dependence of the shell effects on deformations of fission fragments at scission plays the key role in the description of the asymmetry of the fission-fragment mass distribution. With increasing mass number of the fissioning mercury isotope we predicted the evolution of the fission-fragment mass distribution from symmetric for $^{174}$Hg, to asymmetric for isotopes around $^{180}$Hg, and to more symmetric for $^{192,194,196}$Hg. The existence of both symmetric and asymmetric fission modes is expected in the fission of $^{196}$Po. For all fissioning Hg isotopes, the influence of the excitation energy on the shape of the mass distribution was found to be rather weak. In the cases of $^{180,184}$Hg the mass distributions have a pronounced asymmetric shape even at the high excitation energies of the compound nuclei. All these predictions can be checked in the experiments.

This work was supported by RFBR (Moscow) and JINR Grant No. 13-302-01. The IN2P3(France)-JINR(Dubna) and Polish-JINR(Dubna) Cooperation Programmes are gratefully acknowledged.

[1] A. N. Andreyev *et al.*, Phys. Rev. Lett. **105**, 252502 (2010).
[2] J. Elseviers *et al.* (unpublished).
[3] M. G. Itkis, N. A. Kondrat'ev, S. I. Mul'gin, V. N. Okolovich, A. Ya. Rusanov, and G. N. Smirenkin, Sov. J. Nucl. Phys. **53**, 757 (1991).
[4] A. V. Andreev, G. G. Adamian, and N. V. Antonenko, Phys. Rev. C **86**, 044315 (2012).
[5] P. Möller, J. Randrup, and A. J. Sierk, Phys. Rev. C **85**, 024306 (2012).
[6] M. Warda, A. Staszczak, and W. Nazarewicz, Phys. Rev. C **86**, 024601 (2012).
[7] S. Panebianco, J.-L. Sida, H. Goutte, J.-F. Lemaître, N. Dubray, and S. Hilaire, Phys. Rev. C **86**, 064601 (2012).
[8] A. V. Andreev, G. G. Adamian, N. V. Antonenko, S. P. Ivanova, and W. Scheid, Eur. Phys. J. A **22**, 51 (2004).
[9] Sh. A. Kalandarov, G. G. Adamian, N. V. Antonenko, and W. Scheid, Phys. Rev. C **82**, 044603 (2010); **83**, 054611 (2011); Sh. A. Kalandarov, G. G. Adamian, N. V. Antonenko, W. Scheid, and J. P. Wieleczko, *ibid.* **84**, 064601 (2011).